Resolution requirements for velocity gradients in turbulence

By J. Jiménez[1]

1. Motivation

Since high resolution numerical simulations of turbulent flows, or experiments at high Reynolds numbers, represent a substantial investment in resources, the estimation of the minimum resolution required for the study of a given property has been the subject of continued interest. Early results include the papers by Wyngaard (1968, 1969) on the maximum hot wire length allowed for the resolution of the dissipative range of the energy spectrum in isotropic turbulence, and the more recent one by Klewicki and Falco (1990) for wall bounded flows. Both studies conclude that an adequate measurement of the spectrum requires hot wires sensors smaller than approximately three times the Kolmogorov length, $\eta = (\nu^3/\epsilon)^{1/4}$. The latter paper also treats the measurement of velocity gradients and concludes that the same resolution is needed for reliable estimates of the variance of $\partial u/\partial t$, and is probably sufficient for its skewness. From the numerical point of view it has been estimated that the resolution required in a properly de-aliased spectral code for the study of the vorticity structure in the near wall region of a turbulent channel is about 5 Kolmogorov lengths (Kim, Moin and Moser, 1987), although even in that case, the grid spacing in the direction normal to the wall, in which gradients are highest, is usually taken much smaller. The study of the dynamics of intense vorticity structures in isotropic turbulence requires $k_{\max}\eta \geq 2$, where $k_{\max}$ is the largest resolved wavenumber, corresponding to a distance between collocation points $\Delta x/\eta \leq 1.5$ (Jiménez *et al.* 1993).

Different properties require, in general, different resolutions, and the present paper is dedicated to the requirements for the measurement of the probability distribution functions of the velocity gradients and, in particular, of their low order moments. The deviation of these quantities from the values corresponding to a Gaussian distribution was one of the first indications of the presence of Reynolds number-dependent intermittency (Batchelor and Townsend 1949) and has been the object of recent interest as numerical simulations have become able to explore the distribution of gradients in the low Reynolds number range, while new experiments have extended the range to increasingly high Reynolds numbers (Van Atta and Antonia 1980, Saddoughi and Veeravalli 1994). We will use progressive filtering of the results of numerical simulations of isotropic turbulence as a model for the effect of a sensor of finite size (Wyngaard 1968). The numerical issues will be addressed first to insure that the simulations are fully resolved from the point of view of the

1 Also with School of Aeronautics, U. Politécnica, Madrid.

Re_λ	N	$k_{\max}\eta$	$\Delta x/\eta$	$-F_{3\ell}$	$F_{4\ell}$	$F_{6\ell}$	F_{4t}	F_{6t}
66	256	4	0.78	0.47	4.7	60	6.3	120
94	256	2	1.57	0.52	5.3	80	7.6	200

TABLE 1. Numerical and statistical parameters for the cases analyzed in the paper.

velocity gradients. This will also give us an estimate for the numerical resolution required for the different quantities.

2. The numerical fields

The numerical flow fields are the same used in (Jiménez *et al.* 1993) and are extensively discussed there. They are direct numerical simulations of isotropic homogeneous turbulence in triply periodic boxes at two different Reynolds numbers in the low end of the range for which dissipation first becomes independent of Reynolds number. They are summarized in Table 1.

The numerical method is fully spectral, using primitive variables, $\mathbf{u}$, p, with dealiasing achieved by a spherical mask and phase shifting (Rogallo 1981, Canuto *et al.* 1987). The resolution N given in Table 1 reflects the number of real Fourier modes in each direction before dealiasing. A more practical measure of resolution is the largest useful wavenumber after de-aliasing, $k_{\max} = \sqrt{2}N/3$. In terms of distance between "effective" collocation points, the grid spacing is $\Delta x = \pi/k_{\max}$. All simulations are forced to achieve a statistically stationary steady state. Forcing is achieved by introducing, for all the modes with wave numbers $k = |\mathbf{k}| \leq 2.5$, a negative viscosity coefficient whose magnitude is adjusted every few time steps so as to keep constant the product $k_{\max}\eta$. The instantaneous energy dissipation rate, ϵ, the one-component r.m.s. velocity, u', and the Taylor and integral length scales, λ and L, are computed in terms of the three dimensional energy spectrum $E(k)$, as explained in (Jiménez *et al.* 1993). The microscale Reynolds number is defined as $Re_\lambda = u'\lambda/\nu$, and the large-eddy turnover time as $T = L/u'$.

Throughout this paper the probability density functions are often characterized by their generalized flatness factors

$$F_n = \mu_n/\mu_2^{n/2}, \qquad \mu_n = \int y^n p(y)\, dy.$$

Flatness factors with subscript ℓ refer to the pdf of the longitudinal velocity derivatives, $\partial u/\partial x$, while those with subscript t refer to transversal derivatives, $\partial u/\partial y$. In all cases, equivalence was assumed for the three coordinate directions and used to augment the statistics.

The parameters in Table 1 represent the highest resolution available for each Reynolds number. For each run the pdf's of the velocity components and gradients

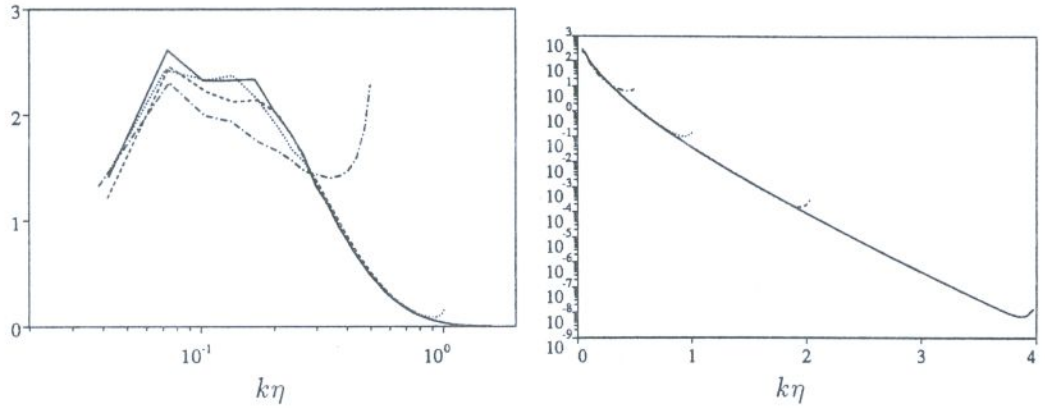

FIGURE 1. Three-dimensional energy spectra for the $Re_\lambda = 66$ simulation at four different resolutions. Left: $\epsilon^{-2/3}k^{5/3}E(k)$, to enhance the "inertial" range. Right: $\epsilon^{-2/3}\eta^{-5/3}E(k)$, to display the dissipation range. ——— : $k_{\max}\eta = 4$, - - - - : 2, ····· : 1, —·— : 0.5.

were computed periodically and accumulated. For all but the highest resolution cases, this was done "on the fly" while the simulation was advanced, and the statistics represent several tens of fields spaced at least by $0.1\,T$. For $N = 256$ the time step was too small to generate a sufficient number of fields in a single simulation, and the statistics were accumulated using the restart files from different runs. The number of fields used in this case is smaller, $O(10)$. The restart fields were also used for the filtering experiments described later.

There is considerable temporal variability in the extreme tails of the distributions, and the values for the different moments given in Table 1 are subject to appreciable statistical uncertainty. The number of significant figures given in the table is intended to give a rough indication of the reliability of the different figures, derived from the variability among different flow fields.

The same simulations were run at lower resolutions to check for numerical convergence. The three dimensional spectra for $Re_\lambda = 62$ at four different values of $k_{\max}\eta$ are given in Fig. 1, and the pdf's for the velocity and for the longitudinal and transverse velocity gradients are given in Fig. 2. It is clear that there is little difference in any of these properties for resolutions better than $k_{\max}\eta \approx 2$, while there is some divergence in the pdf's at $k_{\max}\eta \approx 1$ and a rapid deterioration thereafter. Since higher moments are dominated by the extreme probability tails of the pdf's, Fig. 2d shows that those tails are the first ones affected by the lack of resolution, which is also consistent with the qualitative aspects of the other three parts of Fig. 2. It is noteworthy that even the velocity pdf, which is usually assumed to be dominated by large-scale events, is slightly affected by low resolution. The sub-Gaussian character of that distribution has been observed by other investigators at different Reynolds numbers, and is believed to be real (Anselmet *et al.* 1984, Vincent and Meneguzzi 1991).

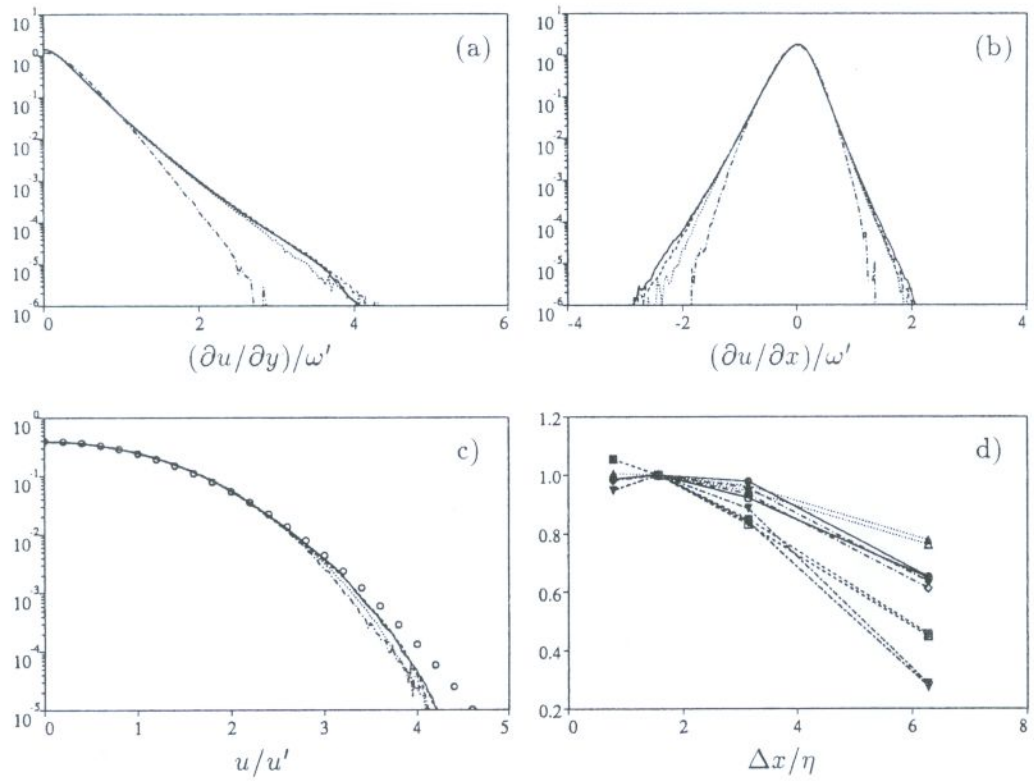

FIGURE 2. Dependence of the probability distributions on numerical resolution. (a-c) Pdf's of velocity and velocity gradients, $Re_\lambda = 66$. Lines are as in Fig. 1 and symbols in (c) are the Gaussian distribution. (d) Dependence of the velocity gradient flatness factors on $\Delta x/\eta = \pi/k_{\max}\eta$. All moments are normalized with their value at $k_{\max}\eta = 2$. $\circ$: $F_{3\ell}$, $\triangle$: $F_{4\ell}$, $\square$: $F_{6\ell}$, $\diamond$: F_{4t}, ∇ : F_{6t}. Solid symbols are $Re_\lambda = 66$, open ones, $Re_\lambda = 92$.

3. Probe size effects

The resolution effects documented above represented a more strict test than the effect of observing the flow with a probe of finite size. While in the former case the dynamics of the small scales are presumably disrupted by the lack of resolution, that is not true in the latter, in which the only effect is a smoothing of "properly computed" quantities. The classical model for the effect of a hot wire of finite length is that in (Wyngaard 1968). It is assumed that the hot wire is only sensitive to one velocity component and that it averages the true velocity signal along its length. No other measurement errors are considered. Whenever a spatial derivative is needed, it is computed as a centered difference from the signal at two neighboring wires. If homogeneous turbulence is assumed and the velocity is represented by its Fourier components,

$$u(\mathbf{x}) = \sum \hat{u}_\mathbf{k}\, e^{i\mathbf{k}\cdot\mathbf{x}},$$

the averaging effect of a hot wire of length h, oriented along z, is equivalent to

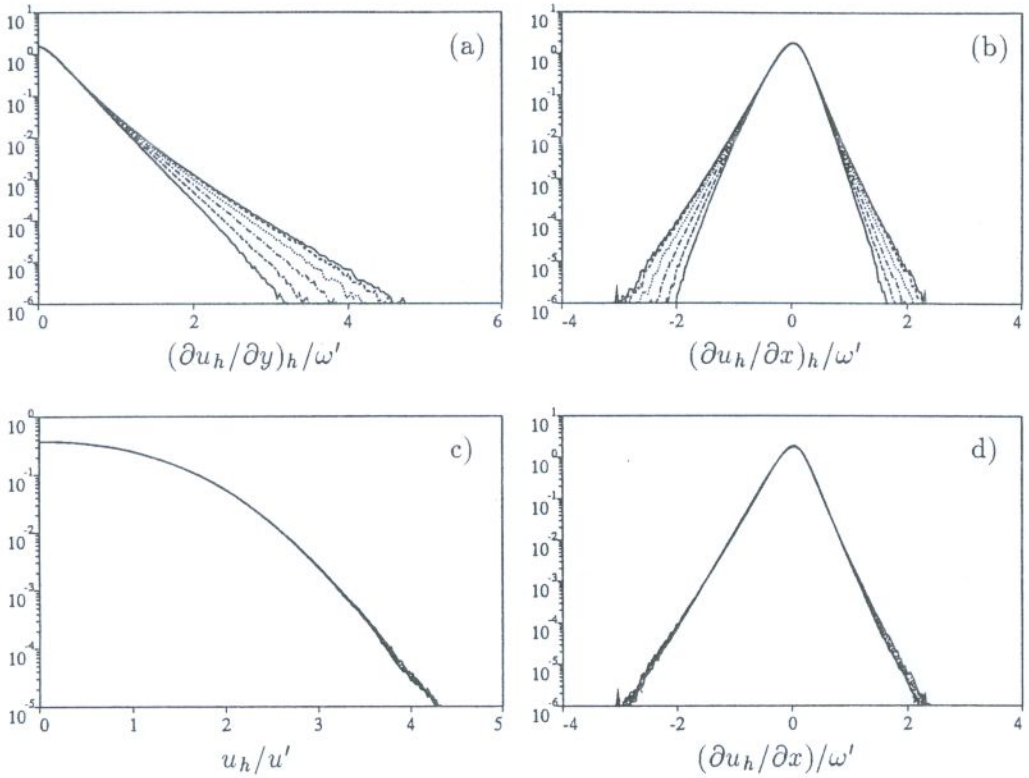

FIGURE 3. Dependence of the probability distributions on experimental resolution. Lines correspond to $h/\eta = 0(1.5)7.5$, in order of decreasing intermittency of distributions. $Re_\lambda = 92$. (a) Filtered transversal derivatives of filtered velocity. (b) Filtered longitudinal derivatives of filtered velocity. (c) Filtered velocity. (d) True longitudinal derivatives of filtered velocity.

multiplying each Fourier components by a filter (Wyngaard 1968)

$$F(\mathbf{k}) = \frac{\sin(k_z h/2)}{k_z h/2}.$$

In the same way, the effect of taking a derivative over a finite distance h is equivalent to multiplying the Fourier components of the derivative by the same filter function (Wyngaard 1969).

We applied this procedures to our numerical fields, using for each Reynolds number the highest available resolution. First the "wire" was oriented along the x-axis and used to obtain filtered values for v and w. The transverse derivatives, $\partial v/\partial z$ and $\partial w/py$, were obtained by filtering the derivatives obtained from the filtered velocities. This was intended to model the effect of two parallel sensors of length h spaced by the same distance. The longitudinal derivatives, $\partial v/\partial y$ and $\partial w/\partial z$, were obtained in two different ways. In experimental practice these derivatives are usually not derived from two separate sensors, but deduced from a single time trace

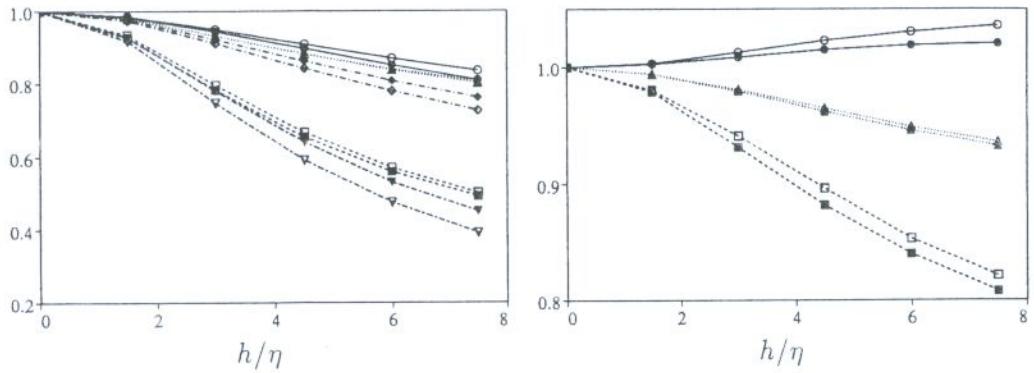

FIGURE 4. Dependence of the velocity gradient flatness factors on the experimental resolution. Left: Filtered derivatives of filtered velocities. Right: True longitudinal derivatives of filtered velocities. Symbols as in Fig. 2d.

using Taylor's approximation. Without taking into account the errors introduced by that procedure, it is in principle possible to sample the time trace fast enough to obtain "true" time derivatives of the signal. The sampling rate is limited by factors such as thermal inertia of the hot wire, seeding density in an LDV signal, or electronic limitations, all of which are essentially unrelated to sensor size. Two sets of longitudinal derivatives were thus obtained. The first one contains "true" derivatives of the filtered velocities, while the second one uses filtered derivatives with a sampling interval h, to make them comparable to the transversal gradients. The whole procedure was repeated with the "wire" oriented along the y and z axis, and pdf's were compiled for all the quantities. The results, as a function of sensor length relative to the Kolmogorov scale, are shown in Figs. 3 and 4.

There are several interesting aspects in those figures. First, as expected, the effect of experimental averaging is somewhat milder than that of numerical underesolution, but the magnitude of the effect is different for the different moments. While the degradation of the sixth order moments is comparable for a wire of length 8η and for a grid pitch of 5η, the third and fourth order moments are never degraded too much by filtering and remain with 20% of their true values even for the longest wire tested in our computations. Also, Wyngaard's criterion for wire length, $h \leq 3\eta$, is seen to be reasonable for the lowest order moments, but to lead to sizable errors for the sixth order flatness.

Perhaps the most unexpected results of Figs. 3 and 4 is the very mild degradation of the longitudinal gradients when only the velocities are filtered while the gradients themselves are computed with spectral accuracy. This indicates that the extreme tails of the pdf's are dominated by events, fronts, or filaments whose size in the direction normal to the gradient is comparatively large. This is of course consistent with modern observations of vorticity filaments in turbulent flows and suggests that reasonably accurate measurements of longitudinal gradients can be obtained by rapid sampling of velocity signals from fairly large sensors.

Another totally unexpected result was the tendency in Fig. 4b for the skewness

of the longitudinal derivatives of the filtered velocity to *increase* with the size of the filter. We have no explanation for this puzzling phenomenon, although it brings to mind the recent observations of persistent skewness in passive scalar fields associated with sharp fronts whose scale is similar to the integral length of the flow (Holtzer and Siggia 1994, Pumir 1994).

4. Conclusions

We have shown that the numerical resolution needed to simulate isotropic turbulence to the level of the sixth moment of the velocity gradient probability distributions is $\Delta x/\eta \approx 1.5$, for properly de-aliased spectral simulations at $Re_\lambda \sim O(100)$.

Using post-processing filtering of fully resolved numerical fields, we have shown that the classical limit on the size of experimental sensors (3η) is sufficient for third or fourth order moments of longitudinal or transverse velocity gradients, but that the sixth order moments require shorter wires. It is shown that most of the degradation in the higher moments results from the discretization of the differential operator and that fairly accurate longitudinal gradients can be obtained from large sensors by rapidly discretizing the time signal. As the discretization distance is extended into the inertial range ($h/\eta \approx 10$), the computation of the gradients merges into that of the normalized structure functions (see Anselmet *et al.* 1984, for a review), whose variation with distance is associated with the intermittency properties of the turbulent field. Our experiments show, however, that the degradation of the higher moments ($n \leq 6$) is substantial even when the discretization distance is kept in the dissipation range.

Finally, we have observed that the skewness of the filtered fields tends to increase with decreasing resolution, suggesting a large-scale origin for this quantity.

Acknowledgments

I have benefited from discussions with S. Saddoughi on experimental technique. The simulations were carried out at the Intel hypercube at NASA Ames and at the Paragon at Wright Patterson AFB. Much of the parallel code development is due to A. A. Wray and R. S. Rogallo. Work was funded by the Center for Turbulence Research and by the Office of Naval Research.

REFERENCES

ANSELMET, F., GAGNE, Y. & HOPFINGER, E. J. & ANTONIA, R. A. 1984 High order velocity structure functions in turbulent shear flows. *J. Fluid Mech.* **140,** 63-89.

BATCHELOR, G. K. & TOWNSEND, A. A. 1949 The nature of turbulent motion at large wave numbers. *Proc. Roy. Soc. London.* **A 199,** 238-255.

CANUTO, C., HUSSAINI, M. Y., QUARTERONI, A. & ZANG, T. A. 1987 *Spectral methods in fluid dynamics.* Springer, pp. 85-86.

HOLTZER, M. & SIGGIA, E. D. 1994 Turbulent mixing of a passive scalar. *Phys. Fluids.* **6,** 1820-1836.

JIMÉNEZ, J., WRAY, A., SAFFMAN, P. G. & ROGALLO, R. S. 1993 The structure of intense vorticity in isotropic turbulence. *J. Fluid Mech.* **255,** 65-90.

KIM, J., MOIN, P. & MOSER, R. 1987 Turbulence statistics in fully developed channel flow at low Reynolds number. *J. Fluid Mech.* **177,** 133-166.

KLEWICKI, J. C. & FALCO, R. E. 1990 On accurately measuring statistics associated with small-scale structure in turbulent boundary layers using hot wire probes. *J. Fluid Mech.* **219,** 119-142.

KOLMOGOROV, A. N. 1941 The local structure of turbulence in incompressible viscous fluids a very large Reynolds numbers. *Dokl. Nauk. SSSR.* **30,** 301-305 (see e.g. L. D. Landau & E. M. Lifshitz, 1959, *Fluid mechanics*, Pergamon, pp. 116-123).

PUMIR, A. 1994 A numerical study of the mixing of a passive scalar in three dimensions in the presence of a mean gradient. *Phys. Fluids.* **6,** 2118-2132.

ROGALLO, R. S. 1981 Numerical experiments in homogeneous turbulence. *NASA Tech. Mem.* **81315.**

SADDOUGHI, S. G. & VEERAVALLI, S. V. 1994 Local isotropy in turbulent boundary layers at high Reynolds numbers. *J. Fluid Mech.* **268,** 333-372.

VAN ATTA, C. W. & ANTONIA, R. A. 1980 Reynolds number dependence of skewness and flatness factors of turbulent velocity derivatives. *Phys. Fluids.* **23,** 252-257.

VINCENT, A. & MENEGUZZI, M. 1991 The spatial structure and statistical properties of homogeneous turbulence. *J. Fluid Mech.* **225,** 1-20.

WYNGAARD, J. C. 1968 Measurements of small-scale turbulence structure with hot wires. *J. Physics E: Sci. Instrum.* **1,** 1105-1108.

WYNGAARD, J. C. 1969 Spatial resolution of the vorticity meter and other hot wire arrays. *J. Physics E: Sci. Instrum.* **2,** 983-987.